Manipulating multiple order parameters via oxygen vacancies: The case of $Eu_{0.5}Ba_{0.5}TiO_{3-\delta}$

Weiwei Li *et al.*

Phys. Rev. B **96**, 115105 — Published 6 September 2017

DOI: 10.1103/PhysRevB.96.115105

Manipulating Multiple Order Parameters via Oxygen Vacancies: The case of $Eu_{0.5}Ba_{0.5}TiO_{3-\delta}$

Weiwei Li[1,2,†], Qian He[3,†], Le Wang[4], Huizhong Zeng[5], John Bowlan[6], Langsheng Ling[7], Dmitry A. Yarotski[6], Wenrui Zhang[8], Run Zhao[1], Jiahong Dai[9], Junxing Gu[4], Shipeng Shen[4], Haizhong Guo[4], Li Pi[7], Haiyan Wang[8], Yongqiang Wang[10], Ivan A. Velasco-Davalos[11], Yangjiang Wu[12], Zhijun Hu[12], Bin Chen[13], Run-Wei Li[13], Young Sun[4], Kuijuan Jin[4], Yuheng Zhang[7], Hou-Tong Chen[6], Sheng Ju[9,*], Andreas Ruediger[11], Daning Shi[1], Albina Y. Borisevich[3,*] and Hao Yang[1,*]

[1]*College of Science, Nanjing University of Aeronautics and Astronautics, Nanjing 211106, China*
[2]*Department of Materials Science and Metallurgy, University of Cambridge, Cambridge CB3 0FS, United Kingdom*
[3]*Materials Science and Technology Division, Oak Ridge National Laboratory, Oak Ridge, Tennessee 37831, USA*
[4]*Beijing National Laboratory for Condensed Matter Physics and Institute of Physics, Chinese Academy of Science, Beijing 100190, China*
[5]*State Key Laboratory of Electronic Thin Films and Integrated Devices, University of Electronic Science and Technology, Chengdu 610054, China*
[6]*Center for Integrated Nanotechnologies, MS K771, Los Alamos National Laboratory, Los Alamos, New Mexico 87545, USA*
[7]*High Magnetic Field Laboratory, Chinese Academy of Science, Hefei 230031, China*
[8]*Materials Science and Engineering Program, Department of Electrical and Computer Engineering, Texas A&M University, College Station, Texas 77843-3128, USA*
[9]*College of Physics, Optoelectronics and Energy, Soochow University, Suzhou 215006, China*
[10]*Materials Science and Technology Division, Los Alamos National Laboratory, Los Alamos, New Mexico 87545, USA*
[11]*Institut National de la Recherche Scientifique — Énergie, Matériaux et Télécommunication (INRS-EMT), 1650 Boul. Lionel Boulet, Varennes J3X 1S2 QC, Canada*
[12]*Center for Soft Condensed Matter Physics and Interdisciplinary Research, Soochow University, Suzhou 215006, China*
[13]*Key Laboratory of Magnetic Materials and Devices, Ningbo Institute of Materials Technology and Engineering, Chinese Academy of Science, Ningbo 315201, China*

Controlling functionalities, such as magnetism or ferroelectricity, by means of oxygen vacancies (V_O) is a key issue for the future development of transition metal oxides. Progress in this field is currently addressed through V_O variations and their impact on mainly one order parameter. Here we reveal a new mechanism for tuning both magnetism and ferroelectricity simultaneously by using V_O. Combined experimental and density-functional theory studies of $Eu_{0.5}Ba_{0.5}TiO_{3-\delta}$, we demonstrate that oxygen vacancies create Ti^{3+} $3d^1$ defect states, mediating the ferromagnetic coupling between the localized Eu $4f^7$ spins, and increase an off-center displacement of Ti ions, enhancing the ferroelectric Curie temperature. The dual function of Ti sites also promises a magnetoelectric coupling in the $Eu_{0.5}Ba_{0.5}TiO_{3-\delta}$.

Transition metal oxides (TMOs) are attracting significant attention due to their astonishing variety of technologically important physical properties, such as two-dimensional electron gas (2DEG), colossal magnetoresistance (CMR), and multiferroic behavior, etc [1-3]. Tuning the concentration and distribution of ions and vacancies in TMOs provides a route to create and control new functionalities [4]. For many applications, for better or worse, the functionality of TMOs and thin film devices is strongly affected by the formation and distribution of oxygen vacancies (V_O). For instance, the introduction of V_O causes a displacement of the Fe ions in $(LaFeO_3)_2/(SrFeO_3)$ superlattices, which induces the polar order [5]. V_O also enable room-temperature ferroelectricity in $SrTiO_3$ thin films by manipulating the TiO_6 octahedral tilting around the vacancy site [6]. The electronic properties of these TMOs, especially ABO_3-pervoskite structure, are extremely sensitive to structural distortions consisting of cation displacements, deformations, and rotations in an ideal three-dimensional framework of corner-connected BO_6 octahedra [7,8]. On the other hand, V_O are well known to play a pivotal role in magnetic properties. Biškup *et al.* suggested that ordered V_O are responsible for insulating ferromagnetism in strained epitaxial $LaCoO_{3-\delta}$ films [9]. Similarly, magnetic phenomena were observed at the $SrTiO_3/LaAlO_3$ interface [10,11] and oxygen-deficient bulk $SrTiO_{3-\delta}$ crystals [12].

Previous studies have shown that it is possible to manipulate the functionality of TMO materials by controlling one order parameter at a time through the concentration or spatial distribution of V_O. A natural question arises whether a single experimental parameter, V_O, has the ability to simultaneously control multiple order parameters, such as both magnetism and ferroelectricity. In particular, multiferroics with ferromagnetic-ferroelectric (FM-FE) coupling are highly promising for fundamental research and practical applications [13-15]. They are scarce, however, due to the near-incompatibility of the formation of magnetic order (partial filled *d*-orbitals in 3*d* TMOs) and the conventional off-centering mechanism of ferroelectricity (empty *d*-orbitals in 3*d* TMOs) within a single phase [16]. Takahiro *et al* demonstrated theoretically that atomic-size multiferroics emerges in nonmagnetic ferroelectric $PbTiO_3$ through V_O formed at surfaces [17]. While, there are few experimental reports about V_O manipulating magnetism and ferroelectricity in the thin films simultaneously. On the other hand, one can engineer multiferroic properties in ABO_3 oxides by chemically controlling the functionality on a site-by-site basis, such as A-site cations providing ferroelectricity and B-site cations supplying magnetism or vice verse. Well known, $BiFeO_3$ (BFO) is the case that ferroelectricity is originated from Bi^{3+} $6s^2$ lone-pair electrons hybridized with O^{2-} $2p^6$ at A-site and antiferromagnetism is derived from Fe^{3+} $3d^5$ at B-site [18]. Unfortunately, the calculations demonstrated that V_O cannot significantly affect the electric polarization, but can slightly alter the value of the macroscopic magnetization of the BFO [19]. The ionic displacements are insensitive to V_O, which is responsible for the unaffected electric polarization.

In this letter, we report a new pathway towards a realization of manipulating magnetism and ferroelectricity simultaneously by using V_O. Based on previous reports, the criterions that a material must satisfy for this proposed mechanism are as follow: (1) the magnetic and electric ordering should originate from different cations, (2) the ionic displacement should be sensitive to V_O. In bulk, $Eu_{0.5}Ba_{0.5}TiO_3$ (EBTO) with a typical ABO_3-perovskite structure shows antiferromagnetic (AFM, T_N ~ 1.9 K) and ferroelectric (FE, T_C ~ 213 K) [20,21]. The AFM and FE are stemmed from the Eu^{2+} $4f^7$ unpaired electrons at A-site and the off-center Ti^{4+} $3d^0$ at B-site, respectively. Moreover, EBTO is structurally similar to the archetypal TMOs, such as $BaTiO_3$ (BTO) and $SrTiO_3$ (STO), and the introduction of V_O has been shown to enhance the ferroelectricity of STO [6,22]. Additionally, our previous results established that the doping of V_O shows strong influence on the magnetic ordering of the $Eu_{0.5}Ba_{0.5}TiO_{3-\delta}$ ($EBTO_{3-\delta}$) thin films [23].

Our present work shows that careful manipulation of V_O can improve both magnetic and FE properties in $EBTO_{3-\delta}$. We experimentally observed that the ferroic orders in $EBTO_{3-\delta}$ thin films are transformed from AFM-FE to FM-FE, and the FE Curie temperature is enhanced to be over room temperature. A small magnetodielectric response was also detected in the V_O doped film, revealing the existence of magnetoelectric coupling. First-principle calculations revealed that the introduction of V_O induces defect associated effects including spin-polarized Ti^{3+} ions, mediating a FM coupling between the local Eu^{2+} $4f^7$ spins, and an enhanced off-center displacement of Ti ions, stabilizing the ferroelectric phase and thus increasing the Curie temperature. The tuning of magnetism and ferroelectricity is both through the medium of Ti sites, which is the origin of the magnetoelectric coupling in $EBTO_{3-\delta}$.

Pulsed laser deposition was used to fabricate $EBTO_{3-\delta}$ films on (001) $SrTiO_3$ (STO) and (001) Nb-doped $SrTiO_3$ (Nb-STO, Nb: 0.5wt%) substrates. All of the $EBTO_{3-\delta}$

films were grown under identical deposition conditions, except for the oxygen pressure, which varied from 1×10^{-1} to 1×10^{-4} Pa (see Supplemental Material for more details [24]). Four kinds of $EBTO_{3-\delta}$ films with different content of V_O, grown at oxygen pressure of 1×10^{-1}, 1×10^{-2}, 1×10^{-3}, and 1×10^{-4} Pa, were named as Sample A, B, C, and D, respectively. Moreover, X-ray reciprocal space maps were measured to confirm that strain created by the lattice mismatch of $EBTO_{3-\delta}$ and Nb-STO is fully relaxed (not shown).

To quantitatively determine the stoichiometry and oxygen concentration of the $EBTO_{3-\delta}$ films, we used nuclear resonance backscattering spectrometry (NRBS). The cation ratio in the $EBTO_{3-\delta}$ films (Eu: Ba: Ti) was revealed to be 1 :1 :2. According to the concentrations of the cations and O, the atomicity of O is estimated to be 2.98, 2.96, 2.91, and 2.85 for Samples A, B, C, and D, respectively (see Fig. S1 of Supplemental Material [24]). By comparing the ideal and real atomicity of O, the content of V_O (δ) is calculated to be 0.02, 0.04, 0.09, and 0.15 in Samples A, B, C, and D, respectively. X-ray photoemission spectroscopy (XPS) was used in consideration of very sensitive to variations in the valence state of transition metal ions. The Eu 4*d* and Ba 3*d* spectra exhibit typical Eu^{2+} and Ba^{2+} features, while both Ti^{3+} and Ti^{4+} are observed in Ti 2*p* spectra (see Fig. S2 of Supplemental Material [24]). It is straightforward that Ti^{3+} has one electron at 3*d* orbital (Ti^{3+}: $1s^2\,2s^2\,2p^6\,3s^2\,3p^6\,4s^0\,3d^1$), indicating the appearance of Ti^{3+} $3d^1$ states in the $EBTO_{3-\delta}$ films. The presence of the Ti^{3+} $3d^1$ state is consistent with the density-functional theory (DFT) calculations and is believed to have contributed to the FM ordering in the $EBTO_{3-\delta}$ films (see below).

Figure 1(a) and 1(b) show the magnetization versus magnetic field for Samples C and D, respectively. Similar results have also been obtained for Samples A and B (see Fig. S3 of Supplemental Material [24]). Pronounced hysteretic loops are observed, consistent with ferromagnetism, having coercivity of 75.3 and 73.5 Oe for Samples C and D, respectively. Note that the derivative of the magnetization shown as insets has a minimum at around 1.85 K, identified as the FM Curie temperature (T_C). In addition, the field dependent magnetization curves are also measured at a higher magnetic field and temperature of 1, 1.5, and 5 K (see Fig. S3 of Supplemental Material [24]). The saturation magnetization, obtained at 1 K, is about 6.72 and 6.80 μ_B/Eu for Samples C and D, respectively, which is close to the ideal magnetic moment of Eu^{2+} ions (7μ_B/Eu).

To further understand V_O effects on magnetic properties, the V_O dependence of coercivity and saturation magnetization are shown in Fig. 1(c). Assuming the local anisotropy energy of ferromagnetism doesn't change significantly with varying the concentration of V_O and according to the Zeeman energy being equal to the anisotropy energy, $E_a = H_c M_s$, the coercivity (H_C) gradually decreases with increasing saturation magnetization from Samples A to D. These results demonstrate that the $EBTO_{3-\delta}$ films become ferromagnetism at low temperatures, in contrast to the antiferromagnetism of bulk EBTO. In addition, there is a possibility that the $EBTO_{3-\delta}$ films with even less V_O are also showing ferromagnetism.

To investigate the V_O effects on ferroelectric properties of $EBTO_{3-\delta}$ films, we performed the temperature-dependent optical second harmonic generation (SHG). Optical SHG signals are plotted versus temperature for four samples in Fig. 2(a).

Clearly, from Samples A to D, the transition temperature increases from 260 to 395 K, which is significantly larger than that of bulk EBTO (~ 213 K). To further confirm the huge enhancement of the FE T_C, we also attempted to measure temperature-dependent dielectric permittivity (see Fig. S4 of Supplemental Material [24]). The curves distinctly show a shift of the maximum in the permittivity (FE T_C) from around 255 K for Sample A to 435 K for Sample D. The trend is consistent with SHG results (see Fig. S5 of Supplemental Material [24]), reflecting that the increase in the content of V_O enhances the FE T_C of $EBTO_{3-\delta}$ films. Due to the introduction of V_O, the peak in permittivity clearly exhibits a frequency dispersion, which is probably a huge influence of Maxwell-Wagner relaxation derived from the leakage current.

Ferroelectric hysteresis loops were also recorded (see insets of Fig. S4 of Supplemental Material [24]), confirming the ferroelectricity of $EBTO_{3-\delta}$ films. The value of saturated polarization at 150 K is about 14 μC cm^{-2}, which is almost twice of that of bulk EBTO (~8 μC cm^{-2} at 135 K) [20]. Additionally, the amplitude and phase images of the piezoelectric response measured at 300 K for Sample D were acquired [Fig. 2(b)]. Stable ferroelectric domains with opposite polarization can be written by applying a dc bias to the AFM tip, suggesting room-temperature ferroelectricity and robust polarization. Similar results have also been observed in Samples A to C (see Fig. S4 of Supplemental Material [24]). Moreover, room-temperature piezoresponse hysteresis loops (PHLs) were also obtained and shown in Fig. 2(c). Almost 180° phase contrast is observed in the phase-voltage PHLs, indicating polarization switching. Associated with phase reversal, butterfly shaped amplitude-voltage loops are also observed. The combination of these results proves that the oxygen-deficient $EBTO_{3-\delta}$ films preserve ferroelectricity. Remarkably, the FE T_C was enhanced to be above room temperature, which makes $EBTO_{3-\delta}$ films attractive for the practical applications [25].

Considering the similarity of lattice structure between EBTO and BTO, the ferroelectricity in EBTO is believed to derive from the off-center displacement of Ti ions [20,21,26]. To further confirm the origin of room temperature ferroelectricity in the $EBTO_{3-\delta}$ films, aberration corrected scanning transmission electron microscopy (STEM) measurements were conducted to analyze the off-center displacement of Ti ions in the $EBTO_{3-\delta}$ films. High angle annular dark field (HAADF) imaging in STEM, also known as Z-contrast imaging [27], can be used to precisely measure cation column locations, from which local cation displacement (related to polarization) can be mapped out unit cell by unit cell [28]. The STEM results for Sample D are shown as Fig. 3. An overview of the $EBTO_{3-\delta}$ film is shown in Fig. 3(a), indicating that the film has consistent thickness and uniform appearance on this scale. Close-up looks reveal that some defects have developed in the film. Figure 3(b) shows a medium angle annular dark field (MAADF) image of the region highlighted in Fig. 3(a), in which bright contrast can be seen in the film and at the interface. Since MAADF is sensitive to small lattice distortions [29], such contrast could be from grains in the specimen thickness direction along the electron beam, which are slightly misoriented with each other due to presence of defects such as dislocations. In order to reliably measure displacements of Ti ions, HAADF images were taken in the areas away from those defective areas, where no MAADF contrast can be seen. The cation column positions, determined using a center-of-mass refinement method, were used to calculate the displacements [Fig. 3(c)]. The HAADF image and the resultant Ti ions displacement map for the $EBTO_{3-\delta}$ film and the STO substrate are shown in Fig. 3(d)-3(f) and 3(g)-3(i), respectively. From the displacement maps, it can be seen that the $EBTO_{3-\delta}$ film has non-zero Ti ions displacements in the in-plane (d_x) and the out-of-plane (d_y) directions. While the absolute value of the displacements is fairly small and approaches the detection limit for the technique, the histogram shown in Fig. 3(j) shows unambiguously that the average value of d_x (blue) and d_y (black) for the $EBTO_{3-\delta}$ film is distinct from zero, namely about 0.07 Å and 0.03 Å, respectively. This finding is consistent with the SHG and PFM results confirming that the FE T_C of Sample D is above room temperature. In contrast to that, the average value of d_x (red) and d_y (green) for the STO substrate (calculated the same way) is about zero, which is consistent with its room temperature paraelectricity.

To understand the physical process underlying the manipulation of multiple order parameters in the $EBTO_{3-\delta}$ films, DFT calculations were performed. A-type atomic arrangement of Eu and Ba ions was used in the calculations due to the simultaneous lowest energy and AFM-FE (see Fig. S6 of Supplemental Material [24]). To further shed light on V_O effects, electron distribution under different configurations of V_O position (see Fig. S7 of Supplemental Material [24]) is investigated and shown in Fig. 4(a). The change of electron distribution around Ti sites is clearly observed upon the presence of V_O, indicating the appearance of Ti^{3+} $3d^1$ states. While, the valence states of Eu and Ba ions remain divalent. Differential charge distribution between AFM and FM orders is also shown in Fig. 4(b). The electron around oxygen and Eu sites show spatially asymmetric variation. In particular, when V_O is located at TiO_2 plane, the electron distribution around Eu sites shows obvious differences between each other, implying a hybridization of Eu^{2+} $4f^7$ and Ti^{3+} $3d^1$. Note that the FM states of all V_O configurations are energetically more favorable than their AFM states [Fig. 4(b)].

Based on the results given above, we now focus on understanding the effects of V_O on FM and FE orders by presenting a model and a band diagram [Figure 4(c) and 4(d), respectively]. Before taking into account V_O, superexchange coupling between Eu^{2+} $4f^7$ spins via Ti^{4+} $3d^0$ states and off-center displacement of Ti ions are responsible for AFM and FE orders observed in bulk EBTO [20,21,30], respectively [Fig. 4(c)]. Combined with XPS valence band spectra [30,31], the existence of V_O creates Ti^{3+} $3d^1$ defect states, localizing within the band gap and overlapping with Eu^{2+} $4f^7$ states [Figure 4(d)]. In this case, the spin-polarized Ti^{3+} will mediate FM coupling between the localized Eu^{2+} $4f^7$spins in $EBTO_{3-\delta}$ [Fig. 4(c)]. Furthermore, at the presence of V_O, Ti ions with remaining oxygen form pyramid structure instead of oxygen octahedra (see Fig. S7 of Supplemental Material [24]) and increase the $d_{3z^2-r^2}$ or d_{xy} character of local orbitals of Ti^{3+} ions adjacent to the V_O sites [32,33]. When V_O is situated in the EuO or BaO plane, Ti ions move naturally towards V_O to avoid electrostatic interaction and the $d_{3z^2-r^2}$ occupation can lead to a local polar distortion. On the other hand, when V_O is placed in the TiO_2 plane, d_{xy} orbital is preferred, resulting in an additional polar distortion in the TiO_2 plane. These local distortions should couple with globe polar distortion in pristine EBTO and will afford a totally new degree of freedom to tune the ferroelectricity in

$EBTO_{3-\delta}$. In other words, the off-center displacement of Ti ions will be enhanced by the introduction of V_O, thereby enhancing the FE Curie temperature in $EBTO_{3-\delta}$ [Fig. 4(c)]. These results definitely approve that tuning V_O can effectively change magnetic and electric degrees of freedom in $EBTO_{3-\delta}$ simultaneously. More than this, it should be emphasized that the manipulating of magnetism and ferroelectricity is both through the medium of Ti sites, revealing the existence of magnetoelectric coupling in $EBTO_{3-\delta}$. The coupling between electric and magnetic orders was confirmed in the V_O doped film by the magnetodielectric measurements [Fig. 5]. Due to the spin-phonon coupling, as shown in Fig. 5(a), the dielectric constant shows a dependence on the external magnetic fields in the FM-FE state [34-36]. In contrast, as shown in Fig. 5(b), the influence of magnetic field is almost negligible in the PM-FE state.

In conclusion, a new mechanism is proposed for controlling multiple order parameters simultaneously by using a single experimental parameter, V_O. $EBTO_{3-\delta}$ was chosen to realize this strategy because magnetism and ferroelectricity are originated from different cations and the off-center displacements of Ti ions are sensitive to V_O. The emergence of ferromagnetism is the result of oxygen vacancy-created Ti^{3+} $3d^1$ defect states, mediating ferromagnetic coupling between the localized Eu $4f^7$ spins. On the other hand, the introduction of V_O increases an off-center displacement of Ti ions, enhancing the ferroelectric Curie temperature of $EBTO_{3-\delta}$. The dual function of Ti sites induces magnetoelectric coupling, which reinforces the high potential of oxygen vacancies engineering as a tool for designing oxide thin films suitable for multifunctional device applications.

The authors thank Kelvin H. L. Zhang for valuable discussion, and also acknowledge the support of the National Basic Research Program of China (No. 2014CB921001), the National Natural Science Foundation of China (Grant No. 11274237, U1632122, 11004145, 51202153, U1332209, U1435208, 11134012, 11174355, 11474349, and 11227405), and the Program for Postgraduates Research Innovation in University of Jiangsu Province under No. CXZZ13_0798. The STEM studies (QH and AYB) is supported by the U.S. Department of Energy, Office of Science, Basic Energy Sciences, Materials Sciences and Engineering Division. The TEM studies at Texas A&M University is funded by the U.S. National Science Foundation (DMR-1643911 and DMR-1565822). Ion beam analysis (YW) and SHG measurements are supported by the Center for Integrated Nanothechnologies (CINT), a US DOE Nanoscale Research Center, jointly operated by Los Alamos and Sandia National laboratories. AR gratefully acknowledges financial support from NSERC through a discovery grant, from FRQNT and from CFI through the leaders opportunity fund.

†W. Li and Q. He contributed equally to this work.

*Corresponding authors:
yanghao@nuaa.edu.cn; albinab@ornl.gov; jusheng@suda.edu.cn

References

[1] A. Ohtomo and H. Y. Hwang, Nature (London) **427**, 423 (2004).

[2] K.-I. Kobayashi, T. Kimura, H. Sawada, K. Terakura, and Y. Tokura, Nature (London) **395**, 677 (1998).

[3] J. Wang *et al.*, Science **299**, 1719 (2004).

[4] S. A. Kalinin and N. A. Spaldin, Science **341**, 858 (2013).

[5] R. Mishra, Y.-M. Kim, J. Salafrance, S. K. Kim, S. H. Chang, A. Bhattacharya, D. D. Fong, S. J. Pennycook, S. T. Pantelides, and A. Y. Borisevich, Nano Lett. **14**, 2694 (2014).

[6] J. Y. Son, J.-H. Lee, and H. M. Jang, Appl. Phys. Lett. **103**, 102901 (2013).

[7] A. M. Glazer, Acta Cryst. B **32**, 3384 (1972).

[8] A. M. Glazer, Acta Cryst. A **31**, 756 (1975).

[9] N. Biškup, J. Salafranca, V. Mehta, M. P. Oxley, Y. Suzuki, S. J. Pennycook, S. T. Pantelides, and M. Varela, Phys. Rev. Lett. **112**, 087202 (2014).

[10] N. Pavlenko, T. Kopp, E. Y. Tsymbal, G. A. Sawatzky, and J. Mannhart, Phys. Rev. B **85**, 020407(R) (2012).

[11] J. A. Bert, B. Kalisky, C. Bell, M. Kim, Y. Hikita, H. Y. Hwang, and K. A. Moler, Nat. Phys. **7**, 767 (2011).

[12] W. D. Rice, P. Ambwani, M. Bombeck, J. D. Thompson, G. Haugstad, C. Leighton, and S. A. Crooker, Nat. Mater. **13**, 481 (2014).

[13] W. Eerenstein, N. D. Mathur, and J. F. Scott, Nature (London) **442**, 759 (2006).

[14] R. Ramesh and N. A. Spaldin, Nat. Mater. **6**, 21 (2007).

[15] N. A. Spaldin, S. W. Cheong, and R. Ramesh, Phys. Today **63**, 38 (2010).

[16] N. A. Hill, J. Phys. Chem. B **104**, 6694 (2000).

[17] T. Shimada, J. Wang, Y. Araki, M. Mrovec, C. Elsässer, and T. Kitamura, Phys. Rev. Lett. **115**, 107202 (2015).

[18] G. A. Smolenskii and I. E. Chupis, Sov. Phys. Usp. **25**, 475 (1982).

[19] C. Ederer and N. A. Spaldin, Phys. Rev. B 71, 224103 (2005).

[20] K. Z. Rushchanskii *et al.*, Nat. Mater. **9**, 649 (2010).

[21] V. Goian, S. Kamba, D. Nuzhnyy, P. Vaněk, M. Kempa, V. Bovtun, K. Knížek, J. Prokleška, F. Borodavka, M. Ledinský, and I. Gregora, J. Phys.: Condens. Matter **23**, 025904 (2011).

[22] M. Choi, F. Oba, and I. Tanaka, Phys. Rev. Lett. **103**, 185502 (2009).

[23] W. Li *et al.*, Sci. Rep. **3**, 2618 (2013).

[24] See Supplemental Material for additional data and analysis of results in this letter.

[25] J. F. Scott, Nat. Mater. **6**, 256 (2007).

[26] R. E. Cohen, Nature (London) **358**, 136 (1992).

[27] S. J. Pennycook and P. D. Nellist, *Scanning Transmission Electron Microscopy: Imaging and Analysis* (Springer, New York, **2011**).

[28] H. J. Chang, S. V. Kalinin, A. N. Morozovska, M. Huijben, Y.-H. Chu, P. Yu, R. Ramesh, E. A. Eliseev, G. S. Svechnikov, S. J. Pennycook, and A. Y. Borisevich, Adv. Mater. **23**, 2474 (2011).

[29] Z. H. Yu, D. A. Muller, and J. Silcox, J. Appl. Phys. **95**, 3362 (2004).

[30] H. Akamatsu, Y. Kumagai, F. Oba, K. Fujita, H. Murakami, K. Tanaka, and I. Tanaka, Phys. Rev. B 83, 214421 (2011).

[31] M. Hoinkis *et al.*, Phys. Rev. B **72**, 125127 (2007).

[32] M. Choi, F. Oba, Y. Kumagai, and I. Tanaka, Adv. Mater. **25**, 86 (2012).

[33] T. Shimada, J. Wang, Y. Araki, M. Mrovec, C. Elisässer, and T. Kitamura, Phys. Rev. Lett. **115**, 107202 (2015).

[34] T. Katsufuji and H. Takagi, Phys. Rev. B **64**, 054415 (2001).

[35] H. Wu, Q. Jiang, and W. Z. Shen, Phys. Rev. B **69**, 014104 (2004).

[36] C. J. Fennie and K. M. Rabe, Phys. Rev. Lett. **97**, 267602 (2006).

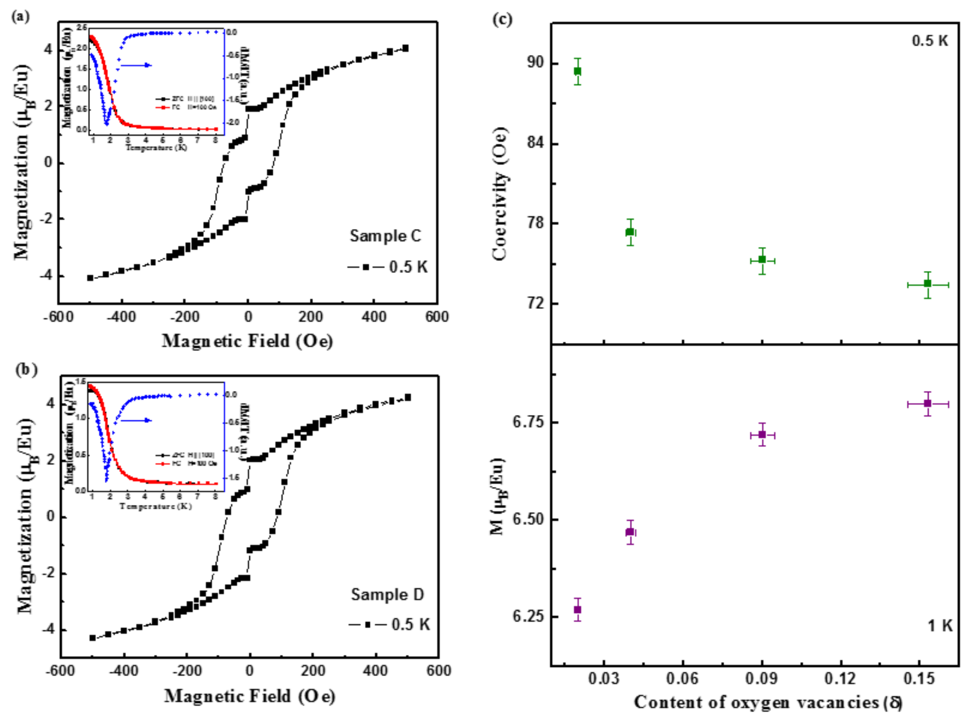

Figure 1 Magnetic hysteresis loops for Sample (a) C and (b) D. Insets show temperature dependence of magnetization curves and the derivative of magnetization with respect to the temperature (obtained from FC curves). (c) The content of V_O (δ) dependences of coercivity and saturation magnetization.

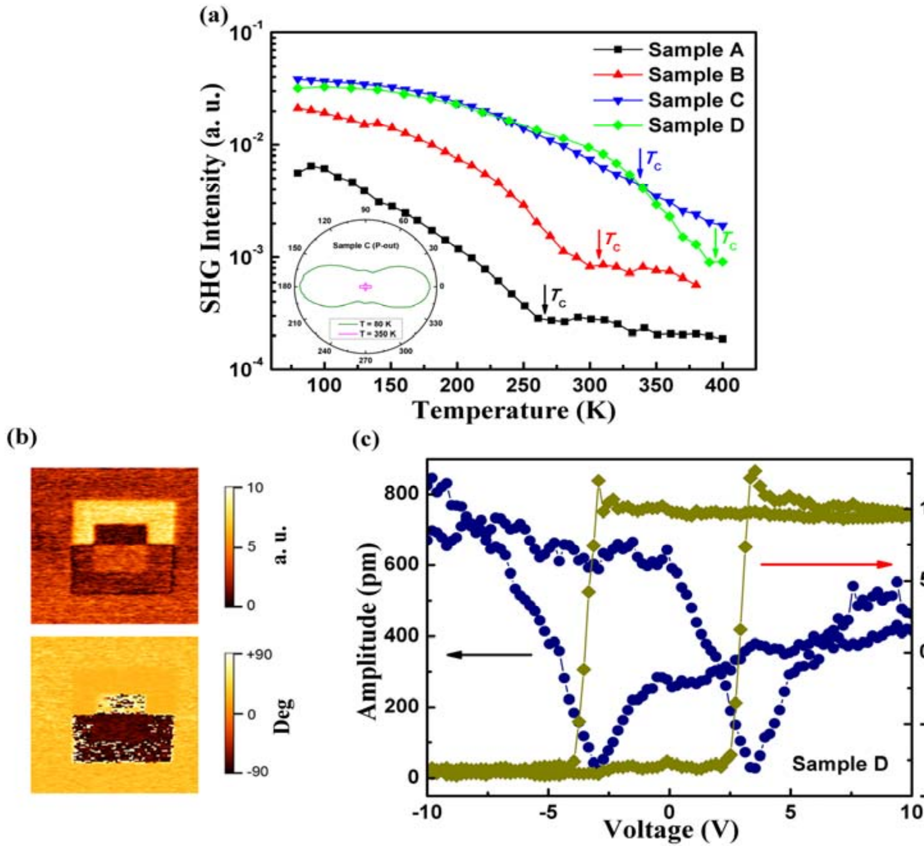

Figure 2 (a) SHG intensity corresponding to the 'P' component of SHG for 'P' polarized fundamental as a function of temperature for Samples A to D. The inset shows polar plot of SHG intensity (radius) versus fundamental polarization (azimuthal angle) at 80 and 350 K for 'P' for Sample C. (b) The PFM amplitude (upper panel) and phase (lower panel) images of the rectangular ferroelectric domain patterns written by a biased tip in Sample D at 300 K. The scan size is 2 μm. (c) Room-temperature piezoresponse amplitude and phase hysteresis loops of Sample D.

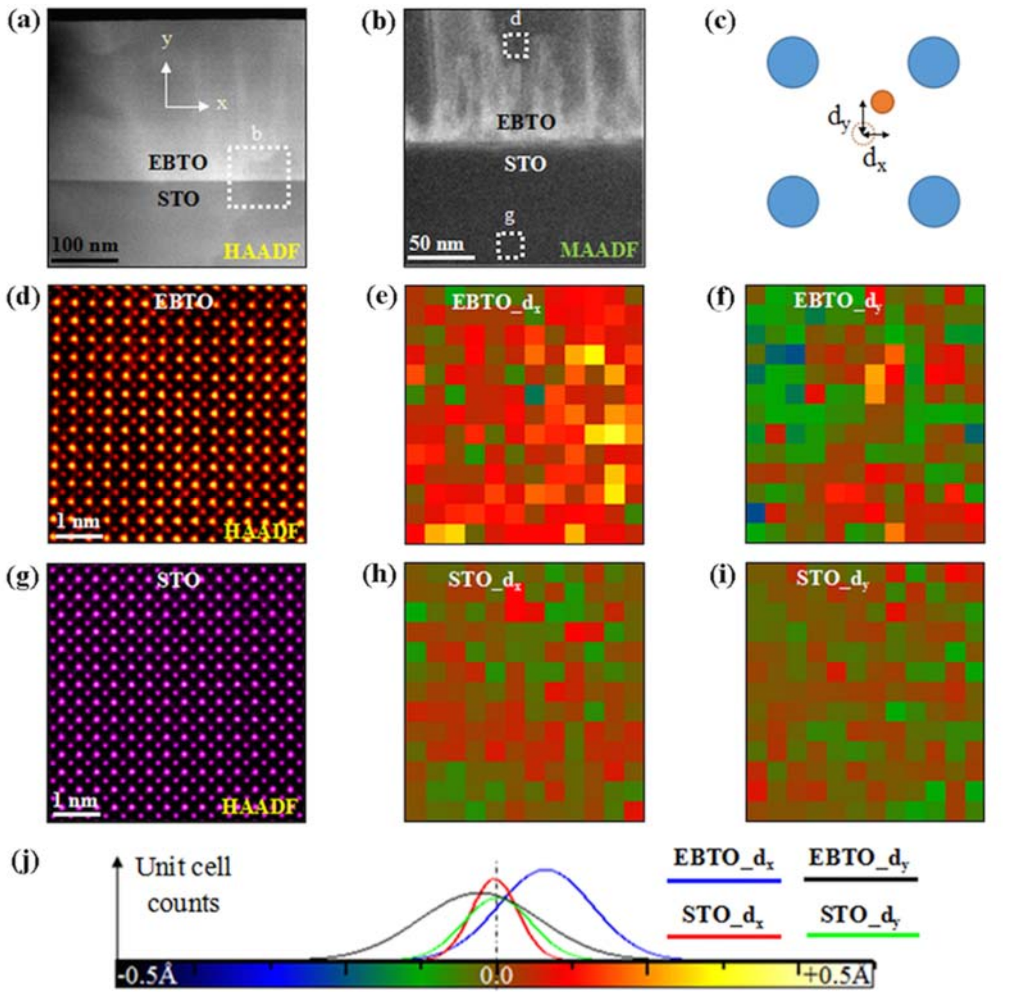

Figure 3 (a) Lower magnification HAADF-STEM image of Sample D. (b) MAADF-STEM image of the highlighted region in (a). (c) Schematic of measuring in-plane (d_x) and out-of-plane (d_y) displacement of B site cations (orange) from the center position with respect to the A site cations (blue). (d-f) Higher magnification HAADF-STEM image of EBTO region highlighted in (b) and the resultant Ti ion displacement map. (g-i) Higher magnification HAADF-STEM image of STO region highlighted in (b) and the resultant Ti ions displacement map. (j) The statistical histogram of Ti ions displacements in (d) and (g), and the color scheme used in the displacement maps.

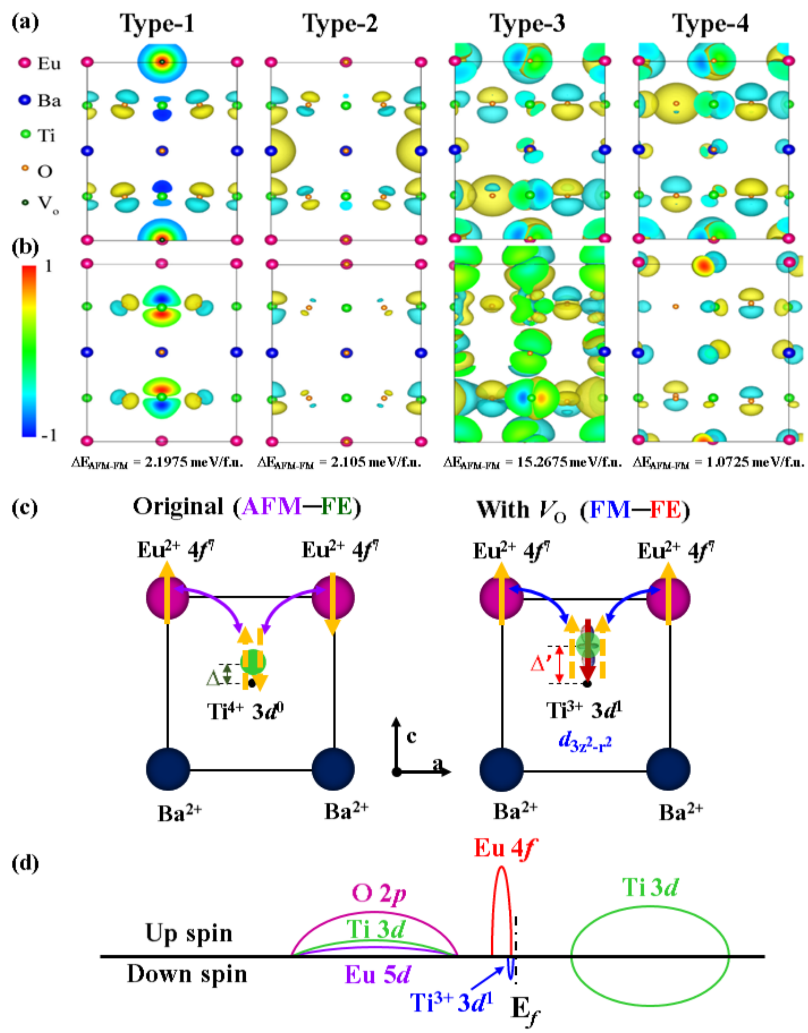

Figure 4 (a) Differential charge upon the presence of V_O. (b) Differential charge between AFM order and FM order of $EBTO_{3-1/4}$. Type-1: V_O at the EuO plane; Type-2: V_O at the BaO plane; Type-3 and Type-4: V_O at the TiO_2 plane. In all cases, FM ordering is favored with the presence of V_O. (c) Sketch of the effects of V_O on ferromagnetism and ferroelectricity in the oxygen-deficient $EBTO_{3-\delta}$. Left panel: Original AFM and FE orders in bulk EBTO. Right panel: FM and FE orders with V_O at the EuO or BaO plane in the $EBTO_{3-\delta}$. (d) Band diagram of the oxygen-deficient $EBTO_{3-\delta}$.

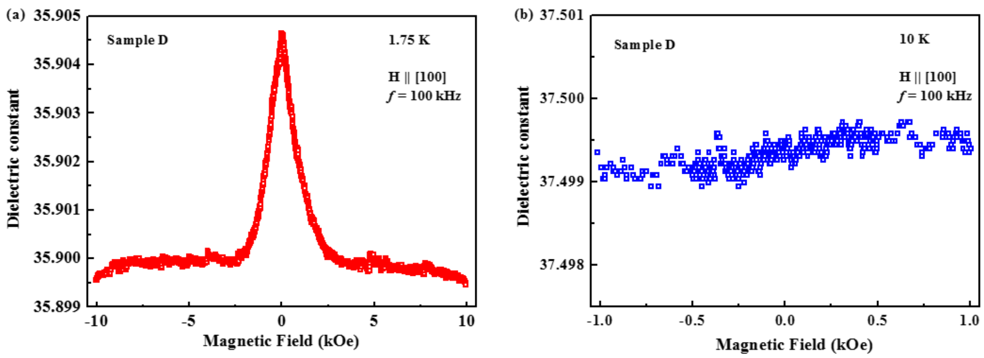

Figure 5 The magnetic field dependence of dielectric constant measured at (a) 1.75 K and (b) 10 K of Sample D.